Clays and Clay Minerals, Vol. 54, No. 1, 1–11, 2006.

FTIR INVESTIGATION OF THE EVOLUTION OF THE OCTAHEDRAL SHEET OF KAOLINITE-SMECTITE WITH PROGRESSIVE KAOLINIZATION

JAVIER CUADROS* AND TERESA DUDEK†

Department of Mineralogy, The Natural History Museum, Cromwell Road, London SW7 5BD, UK

Abstract—Twenty two samples were studied to investigate the nature and evolution mechanism of mixed-layer kaolinite-smectite (K-S). We examined the <2 μm or <0.2 μm fraction of K-S formed by hydrothermal and hypergenic alteration of volcanic material. The samples are from three localities: 20 specimens from a Tortonian clay deposit in Almería, Spain; one specimen from weathered Eocene volcanic ash from the Yucatan Peninsula, Mexico; and one sample from a weathered Jurassic bentonite from Northamptonshire, England. The samples were studied using chemical analysis, X-ray diffraction (XRD) and Fourier transform infrared spectroscopy (FTIR). The XRD patterns of the oriented, glycolated mounts were modeled using NEWMOD and the proportion of smectite and kaolinite layers was determined, ranging between 0 and 80% kaolinite. The analysis of the OH-stretching region of the FTIR spectra at different temperatures (180−550ºC) showed the progressive dehydroxylation of kaolinite domains and, perhaps, of smectite domains, but no detailed information could be obtained about the sequential OH loss in different cation environments. The abundance and short-range ordering of the octahedral cations were studied using the OH-bending bands. The chemical and FTIR-estimated octahedral cation abundances were broadly similar. Aluminum showed a tendency to mix with Fe and Mg rather than to form AlAl pairs. Al-for-Mg substitution accompanying kaolinization was evident from the increase in AlAl pairs and decrease in AlMg pairs. Iron is retained in the structure. No other octahedral cation rearrangement was observed. The intensity of the 750 cm^{-1} band, assigned to translational vibrations of external OH groups in a kaolinitic environment, was quantified and modeled in relation to kaolinite layer proportion. The chemical data show that there are residual interlayer cations in kaolinite domains, which, in accordance with the model mentioned above, disturb external OH-translation vibrations. These results indicate the persistence of certain chemical and structural smectite features in kaolinite domains and thus support a smectite kaolinization process via a solid-state transformation. This confirms previous XRD, thermal, chemical and NMR analyses of the same sample set.

Key Words—Cation Distribution, FTIR, Kaolinite-smectite.

INTRODUCTION

The present contribution follows our recent study of mixed-layer kaolinite-smectite (K-S) (Dudek *et al*., 2006), which integrates the results of XRD, thermogravimetry (TG), chemical analysis and ^{29}Si nuclear magnetic resonance (NMR) to assess the structure and the mechanism of formation and transformation of K-S samples from both hydrothermal and hypergenic settings. We observed non-linear relations between the proportion of kaolinite and smectite layers measured by XRD and other parameters describing different aspects of the structure and chemical composition of K-S, such as percent weight loss due to the dehydroxylation of the octahedral sheet, position of the 06 XRD peak, the area of the kaolinite ^{29}Si NMR peak, MgO and Fe_2O_3 contents, and cation exchange capacity (CEC). Analysis of these trends led us to the conclusion that smectite kaolinization is a solid-state transformation that proceeds through several non-simultaneous stages. The progressive removal of tetrahedra and the increasing abundance of OH groups in the octahedral sheet lead to the development of kaolinite-like patches or domains within smectite layers. However, the development of the patches and their collapse to ~7 Å (as measured by XRD) do not progress simultaneously, because the collapse happens only when the patches acquire sufficient size. Also, other chemical and structural changes that occur during smectite-to-kaolinite transformation, such as Al-for-Mg replacement in the octahedral sheet and Si-for-Al in the tetrahedral sheet, and the resulting removal of interlayer cations, are not immediately linked to the collapse of layers to ~7 Å. We also observed that Fe is either retained in the structure of the newly formed kaolinite or released at a much slower rate than that of the transformation.

In the present paper we describe the results of FTIR applied to the same set of samples. The chief advantage of FTIR is that it gives a direct insight into the cationic environments of the OH groups and allows their qualitative and quantitative assessment.

Previous FTIR studies of K-S provided general qualitative information on the composition of K-S, using FTIR as a tool to detect smectite and kaolinite by tracing the progressive appearance of bands char-

* E-mail address of corresponding author:
J.Cuadros@nhm.ac.uk
† Present address: Institute of Geological Sciences, Polish Academy of Sciences, Senacka 1, Kraków, Poland
DOI: 10.1346/CCMN.2006.0540101

acteristic of these two phases in the OH-stretching region (Churchman *et al*., 1994; Środoń, 1980) or both OH-stretching and -bending regions (Delvaux *et al*., 1989, 1990). They emphasized the importance of the 3700 cm^{-1} OH-stretching vibrations to detect small amounts of kaolinite. However, no attempt was made to extract any further structural information on mixed layering. Madejová *et al*. (2002) performed a quantitative FTIR study of kaolinite dispersed in fine fractions of bentonite and found that the limit of detection of kaolinite is as low as 0.5 mass%. Churchman *et al*. (1994) and Delvaux *et al*. (1990) also discussed the FTIR signatures that help to differentiate between kaolinite and halloysite in mixed-layer sequences with smectite.

In the present study we apply a method of FTIR spectrum decomposition into individual metal-OH-metal bending bands, which allows relatively accurate quantification of cation pairs in the structure and assessment of cation ordering. The FTIR results show a lack of cation rearrangement during the reaction and thus contribute additional evidence for a solid-state transformation as the most likely mechanism of smectite kaolinization.

MATERIALS AND METHODS

The samples investigated in this study represent both hydrothermal and hypergenic alteration of volcanic material. Twenty samples are from a Tortonian clay deposit (Almería, Spain; Linares, 1985), one (RS49) is from a weathered Eocene volcanic ash (Yucatan, Mexico; Schultz *et al*., 1971), and one (CWP-73) from a weathered Jurassic bentonite (Northamptonshire, England; Hillier *et al*., 2002). The two last samples widened the range of K-S composition. The specimens from England and Mexico were pre-treated to remove amorphous Fe phases by the ammonium oxalate (Smith, 1994) and the dithionite-citrate-bicarbonate (Jackson, 1975) methods, respectively. The <2 μm particle size fraction (<0.2 μm for sample RS49) was separated from the bulk samples by dispersion in distilled water and sedimentation according to Stoke's law. The clay separates contain virtually only K-S; trace amounts of quartz were found in four or them. Aliquots of the separated fraction were Li- and Ca-saturated in the exchangeable cation sites by dispersion in 3 M LiCl and 0.1 M $CaCl_2$ solutions, respectively. The solid/liquid ratio was 100 mg/10 mL and the samples were exchanged three to four times.

The XRD analysis was performed at the Natural History Museum (London, UK) using a Philips PW1050 diffractometer operating under the following conditions: 42 kV, 42 mA, Cu tube, graphite secondary monochromator, 1° divergence slit and 0.1 mm receiving slit. The Li-saturated samples were analyzed in oriented mounts prepared by sedimentation on glass slides (2.5 mg/cm^2) and recorded in air-dried and glycolated forms (overnight saturation in ethylene glycol atmosphere at 60ºC) from 3 to 30º2θ, at 0.05º2θ/step and 10 s counting time. The proportion of kaolinite and smectite layers in K-S (percent kaolinite layers, % K) was calculated by fitting the experimental patterns of the ethylene glycol-saturated samples with those calculated with the NEWMOD computer program (Reynolds and Reynolds, 1996).

Chemical analyses, including CEC, of the Los Trancos specimens are from Reyes *et al*. (1978) and Cuadros *et al*. (1994). These analyses were performed before cation exchange. The Mexico and England specimens were analyzed at the Natural History Museum, London, using an ICP-AES Varian Vista Pro apparatus after dilution in $LiBO_2$ (1:5), fusion and dissolution in HNO_3. These two samples were analyzed after cation exchange.

The TG analysis was performed at the Istituto di Metodologie per l'Analisi Ambientale, CNR, Potenza, Italy, using a Seiko Exstar 6000 apparatus. The samples were heated in Al_2O_3 crucibles from 20 to 1050ºC at 10ºC/min in a N_2 flow. Sample weights ranged from 9 to 15 mg. The dehydroxylation weight loss was measured from the TG curves, after discrimination from hydration water loss. For our samples, the temperature of the transition between dehydration and dehydroxylation ranges from ~260 to 400ºC.

We performed two types of FTIR experiments using a Perkin Elmer FTIR system at the Natural History Museum. In the first type, selected samples (representing a range of % K values) were analyzed in the Perkin Elmer AutoImage FTIR microscope equipped with a liquid-nitrogen-cooled mercury cadmium telluride (MCT) detector and a Linkam FTIR heating and cooling stage. A small amount of sample was placed on a ZnSe window, directly on the piece containing a thermopar that controls the temperature. The stage is closed and the IR beam enters and exits it through ZnSe windows. We analyzed single clay particles, thin and large enough to provide a reliable spectrum. The spectra were recorded from the same clay particle at ambient temperature and after heating to the following temperatures: 180−300ºC, 300−350ºC, 420−430ºC, 500ºC and 550ºC. The wide range of the lowest temperature (*i.e*. from 180 to 300ºC) is due to the variable hydration-water content (lowest for the most kaolinitic sample) and ease of water removal (greater for kaolinite-rich K-S). For each sample, 50 scans were recorded in the 4000 to 700 cm^{-1} range in transmittance mode with a resolution of 4 cm^{-1}. The original interest in the heating experiments was based on the fact that dehydroxylation in kaolinite occurs at lower temperatures than in montmorillonite. We expected, therefore, to be able to identify the octahedral composition of smectite and kaolinite domains in K-S through monitoring the gradual loss of the OH groups related to the different cations with increasing temperature. However, we encountered problems that made the attempt unsuccessful. The OH-bending region of the

https://doi.org/10.1346/CCMN.2006.0540101 Published online by Cambridge University Press

spectra from the heated samples was deformed as the SiO band at ~1000 cm^{-1} widened considerably and enveloped the OH bands which thus became almost imperceptible. The OH-stretching region of the spectra was noisy and did not show sufficient detail. The hydration water band that overlaps smectite bands in the OH-stretching region remained up to relatively high temperatures and also complicated the analysis. However, we were able to investigate general changes in the OH-stretching region during the consecutive stages of heating. This was done by subtracting the spectra recorded at higher temperatures from those recorded at the lowest temperature (excluding ambient temperature because the hydration water band was relatively prominent). The product of the subtraction was then decomposed into several bands that correspond to the approximate positions of kaolinite bands (~3700 cm^{-1} and ~3660–3640 cm^{-1}) and smectite bands (~3660–3640 cm^{-1}). The decomposition was performed by curve-fitting, using the computer program Galactic Grams/AI (version 7.01). The areas of the bands in the subtracted spectra were expressed as a fraction of the areas of the individual bands from the spectra recorded at the lowest temperature.

In the second type of experiments, all samples were analyzed as KBr pellets (sample/KBr ratio of: 1 mg/200 mg) using a Perkin Elmer Spectrum One workbench equipped with a deuterated triglycine sulphate (DTGS) detector with a CsI beamsplitter. Spectra were recorded in the range from 4000 cm^{-1} to 300 cm^{-1} with a 5 cm^{-1} resolution, in transmission mode. The region of the OH-bending vibrations (940–550 cm^{-1}) was selected for a detailed analysis because it does not show interference with water hydration bands and because the bands are better resolved. First, a baseline was subtracted as shown in Figure 1. The baseline was calculated using a quintic polynomial function after fixing its value at both sides of the part of the spectrum to be analyzed. There is uncertainty about the accuracy of the position of the baseline. The accuracy of this procedure and the overall analysis is assessed in the results section. The spectra were then deconvoluted in order to find the band maxima and finally decomposed by curve-fitting into the individual metal-OH-metal bands (metal = Al, Mg, Fe) as Gaussian-shaped functions. The intensities of the bands were normalized with respect to the sum of the areas of all OH-bending bands to allow comparison between samples.

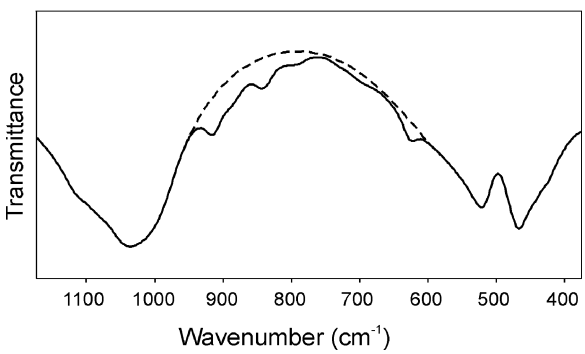

Figure 1. Baseline (dashed) subtracted from the OH-bending region of the original spectrum before its deconvolution and decomposition into single metal-OH-metal bands.

RESULTS AND DISCUSSION

XRD measurements of kaolinite:smectite layer proportion

Table 1 shows the NEWMOD-calculated compositions of K-S samples and the parameters used for the calculations. Selected examples of the XRD experimental and modeled patterns are presented in Figure 2. The % K indicates the percentage of kaolinite layer content in K-S. A satisfactory fit for the peak positions and widths was obtained for all samples. However, we encountered problems with the fitting of the background, especially in the low-angle region. For the most

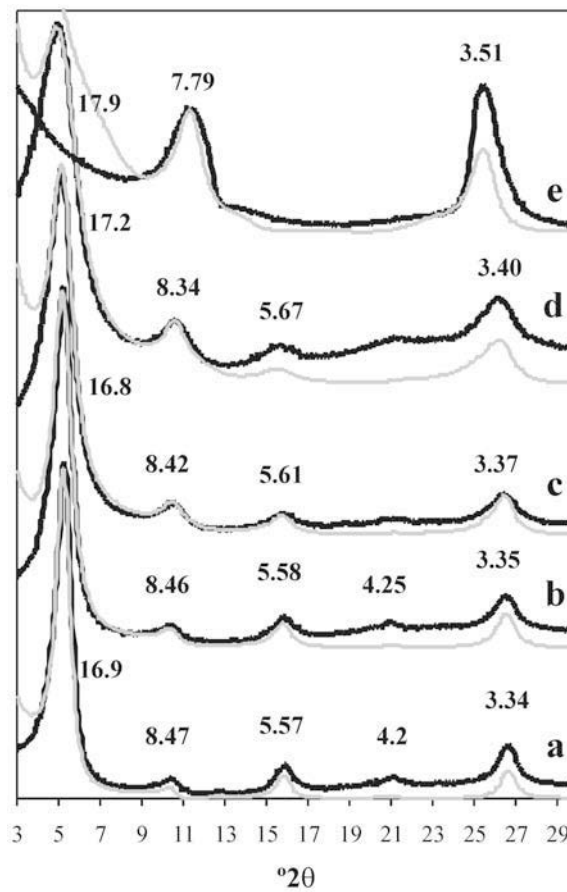

Figure 2. Selected XRD patterns of the oriented, ethylene glycol-solvated K-S samples and their NEWMOD-modeled traces (black: experimental, gray: calculated). Peak positions in Å. (a) smectite (TR-4); (b) 16% K (LT-9/1); (c) 32% K (TR-125); (d) 49% K (TR-121); (e) 80% K (RS49).

https://doi.org/10.1346/CCMN.2006.0540101 Published online by Cambridge University Press

Table 1. The NEWMOD-calculated compositions of the K-S samples (clay fraction) and the parameters used for the modeling.

Sample	Total %K	Phase	%K in each phase	Wt.% of phase	d_K (Å)	N_{ave}	N
TR-4	0	smectite	–	100	–	2.5	1–10
TR-146	0	smectite	–	100	–	2.5	1–10
T-21	7	K–S	7	100	7.4	2.5	1–10
TR-3	7	K-S	7	100	7.4	2.5	1–10
T-16	10	K-S	10	100	7.4	2.5	1–10
TR-2	13	K-S	13	100	7.4	2.5	1–10
LT-9/1	16	K-S	10	90	7.4	2.5	1–10
		K-S	60	10	7.15	2.5	1–10
T-22	25	K-S	13	70	7.4	2.5	1–10
		K-S	50	30	7.4	2.5	1–10
LT-10/6	32	K-S	20	60	7.4	2.5	1–10
		K-S	60	30	7.15	2.5	1–10
		smectite	–	10	–	2.5	1–10
TR-119	32	K-S	20	80	7.4	2.5	1–10
		K-S	70	20	7.15	2.5	1–14
TR-125	32	K-S	15	65	7.4	2.5	1–10
		K-S	60	35	7.15	2.5	1–10
LT-9/3	33	K-S	25	75	7.4	2.5	1–10
		K-S	60	20	7.15	2.5	1–10
TR-115	34	K-S	25	60	7.4	2.5	1–10
		K-S	60	30	7.15	2.5	1–10
		smectite	–	10	–	2.5	1–10
T-18	37	K-S	20	70	7.4	2.5	1–10
		K-S	70	30	7.15	2.5	1–14
TR-117	38	K-S	38	100	7.4	2.5	1–10
LT-9/2	39	K-S	25	55	7.4	2.5	1–10
		K-S	60	35	7.15	2.5	1–10
		smectite	–	10	–	2.5	1–10
T-20	47	K-S	30	70	7.4	2.5	1–10
		K-S	80	30	7.15	2.5	1–14
TR-121	49	K-S	40	85	7.4	2.5	1–10
		K-S	90	15	7.15	2.5	1–14
LT-2	55	K-S	40	75	7.4	2.5	1–10
		K-S	90	25	7.15	2.5	1–14
LT-10/1	61	K-S	30	55	7.4	2.5	1–10
		K-S	90	42	7.15	2.5	1–14
		kaolinite	100	3	7.12	10	1–55
RS49	80	K-S	80	100	7.15	3	1–14
CWP-73	85	K-S	85	90	7.15	2.5	1–14
		Illite	–	10	–	4	1–14

d_K: d value of kaolinite layers; N_{ave} and N: mean number of layers and range of number of layers in the coherent scattering domains. Other parameters used for modeling: d value of ethylene glycol-solvated smectite layers: 16.9 Å for RS49 and CWP-73, 16.7 Å for all the other samples; d value of illite (sample CWP-73): 9.94 Å; ordering: R = 0 except for CWP-73 and RS49 where R = 1; σ* = 30.

kaolinitic samples, RS49 and CWP-73, there is also a misfit in the intensity of the peak around 26º2θ, which we were not able to solve.

For eight samples, there was a good fit of the experimental and theoretical patterns using one phase (smectite or K-S, Figure 2a,e). For the other 12 samples, two or three phases were needed, including K-S of different composition (kaolinite-poor: <50% K, and kaolinite-rich: >50% K), smectite, and, in two cases, kaolinite and illite (Figure 2b–d). K-S with <50% K was a dominant component of the mixtures, comprising 55–90 wt.% (Table 1). This heterogeneity may be related to the differential transformation of smectite to kaolinite within a confined space. However, the model of phase mixing applied to simulate this heterogeneity probably does not represent the exact composition of the corresponding samples.

Some of the calculation parameters for kaolinite-poor and kaolinite-rich K-S were different. The 7.4 Å d spacing of the kaolinitic layers in K-S with <50% K may suggest that they are non-expanding halloysite rather than kaolinite (*e.g.* Brown and Brindley, 1980). We were not able to differentiate between kaolinite and halloysite in K-S, because the available methods (reviewed by

https://doi.org/10.1346/CCMN.2006.0540101 Published online by Cambridge University Press

Theng *et al*., 1984), based on halloysite layer swelling, also cause the expansion of smectite layers, and therefore are not suitable for K-S samples. However, Brindley (1980) suggested that halloysite is a highly disordered form of kaolinite and, in K-S with low kaolinite content, disordered kaolinite layers are more likely to be present than well crystallized kaolinite layers. As it is not possible to discriminate between the two, for simplicity we refer to the 7.4 Å component as kaolinite, in line with many previous studies describing K-S.

The values for the goniometer radius (17.3 cm) and sample length (2.5 cm) from our diffractometer were used in the NEWMOD calculations. The Fe content in smectite was taken from the chemical data, recalculated for the half unit-cell of a 2:1 dioctahedral clay structure. The Fe content of our samples ranges from 0.03 to $0.2/O_{10}(OH)_2$. We assigned all Fe in a given sample to smectite layers, although this appears not to be the case. We found, however, that the patterns calculated using different Fe content (within the range of Fe values in our samples) in smectite and 7 Å layers are identical. Kaolinite layers were calculated without Fe.

FTIR data

OH-stretching region. Figure 3 shows the stretching region (3800–3400 cm^{-1}) of the FTIR spectra (workbench experiments) for selected samples arranged according to increasing % K. As expected, there is a progressive growth of the 3700 cm^{-1} band, corresponding to AlAlOH-stretching vibrations in kaolinite (*e.g.* Russell and Fraser, 1994) with increasing degree of kaolinization. It should be noted that this band was not observed in the samples that are characterized by XRD as pure smectite (TR-4 and TR-146, Table 1). However, according to our TG results, these samples already contain kaolinite domains. Although the 3700 cm^{-1} region is very sensitive to the presence of kaolinite in mineral mixtures (Madejová *et al*., 2002), kaolinite crystals in a physical mixture with smectite are not equivalent to kaolinite-like domains within smectite layers in K-S. Kaolinite-like domains are likely to be affected by the surrounding smectite structure and their 3700 cm^{-1} band can be expected to be less intense than in well crystallized kaolinite. Thus, a number of AlAlOH groups in a kaolinite-like domain in mixed-layer K-S will produce a band of lower intensity than the same number of AlAlOH groups in a kaolinite crystal. It seems, therefore, that TG is more sensitive than XRD and FTIR for detecting kaolinite in K-S.

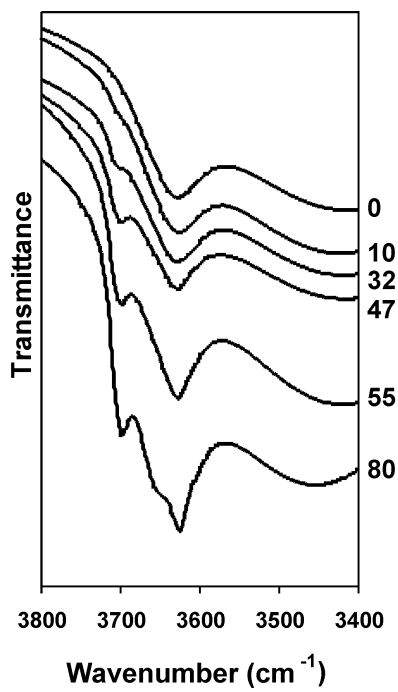

Figure 3. The OH-stretching region of selected samples (TR-4, T-16, TR-119, T-20, LT-2, RS49). The figure shows progressive development of the ~3700 cm^{-1} band and sharpening of the ~3620 cm^{-1} band with increasing kaolinite content in K-S (expressed as % K in the figures at right of the plot).

Churchman *et al.* (1994), Delvaux *et al.* (1990) and Watanabe *et al.* (1992) inferred that the several soil samples they studied had halloysite, rather than kaolinite, interstratified with smectite because they found no band at 3650 cm^{-1}. In our samples, this band only appears in those containing $\geqslant$80% K (Figure 3). In our view, this may be due to a constant increase in crystalline order in the kaolinitic structure with increasing kaolinization, in which the structure progresses from a halloysite-like stage to a disordered kaolinite-like stage, as observed by IR (Russell and Fraser, 1994). Also, the 3650 cm^{-1} band could be masked in the less kaolinitic specimens by the smectite band.

Heating-experiment analysis of the OH-stretching region. The heating experiments were conducted using the microscope on seven samples with a % K range of 0 to 85 (TR-4, TR-119, T-20, TR-121, LT-2, RS49, CWP-73, see Table 1). Figure 4 shows the OH-stretching region of the spectra recorded at the consecutive stages of heating for a sample of intermediate % K content. As expected, due to progressive dehydroxylation, there is a gradual loss of absorption intensity as heating progresses, and the absorption loss seems greater in the ~3700–3600 cm^{-1} region. There is also decreased absorption in the water-hydroxyl region (below 3600 cm^{-1}). In order to evaluate the loss of absorption corresponding to structural hydroxyls we subtracted the spectra recorded at the higher temperatures from that run at the lowest temperature for all samples subjected to the heating experiments. Figure 5 shows two subtracted spectra and their decomposition for sample T-20 (the same as in Figure 4). At 420ºC, the absorption loss occurs at ~3700 cm^{-1}, while at 500ºC it occurs at both ~3700 cm^{-1} and ~3660–3640 cm^{-1} (thick gray lines). In some of the spectra, the ~3660–3640 cm^{-1} region

https://doi.org/10.1346/CCMN.2006.0540101 Published online by Cambridge University Press

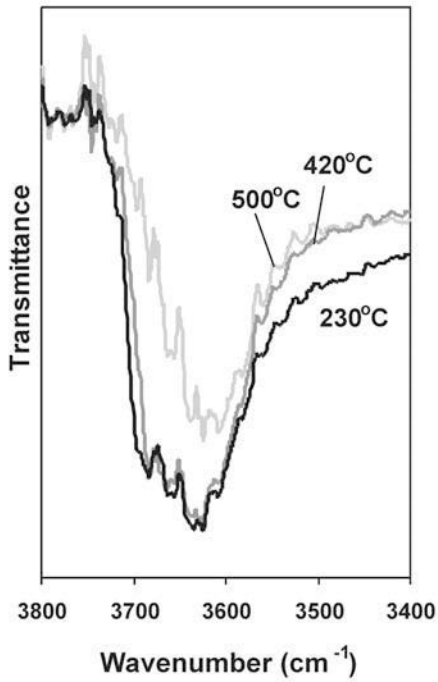

Figure 4. The OH-stretching region of sample T-20 (47% K) recorded at three subsequent stages of heating.

could not be modeled precisely due to the influence of the hydration water bands (thin black lines). Figure 5 is a good example of the results of this procedure: the intensity loss at low temperature occurred only at 3700 cm^{-1} or was higher than that at 3660–3640 cm^{-1}, but at higher temperature the relative amount of intensity loss at 3660–3640 cm^{-1} increased. This is due to the fact that kaolinite dehydroxylates at lower temperature than montmorillonite. Indeed, kaolinite has maxima at 3700 and 3620 cm^{-1} while the smectite maximum is at ~3620 cm^{-1}.

We assessed the absorption loss at the subsequent temperatures by representing the areas of the bands at ~3700 cm^{-1} and at ~3600–3640 cm^{-1} in the subtracted spectra as a fraction of the areas of the individual bands at the lowest temperature. Figure 6 is the result of these calculations and illustrates the evolution of the absorption loss at the consecutive stages of heating for the two regions ~3700 cm^{-1} and ~3660–3640 cm^{-1}. As can be expected, the absorption loss increases with increasing temperature. The fraction of absorption loss for each temperature is always greater in the 3700 cm^{-1} region, indicating that the heating experiments show mainly the progressive dehydroxylation of kaolinite layers in K-S. However, partial smectite dehydroxylation is probably also happening at the higher temperatures. The combination of the absorption loss from both phases is likely to be one of the causes of the

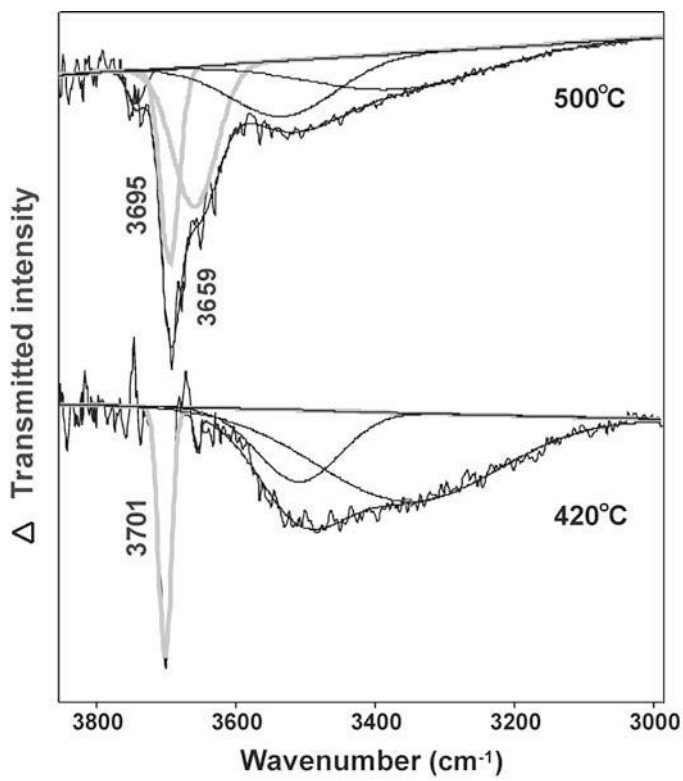

Figure 5. Results of the subtraction of the spectra recorded at 420ºC and 500ºC from that recorded at 230ºC for sample T-20. The spectra are decomposed into several bands: the thick gray lines, labeled with their wavenumber, correspond to kaolinite (~3700 cm^{-1}) and kaolinite plus smectite (~3660 cm^{-1}); the thin black lines correspond to hydration water.

https://doi.org/10.1346/CCMN.2006.0540101 Published online by Cambridge University Press

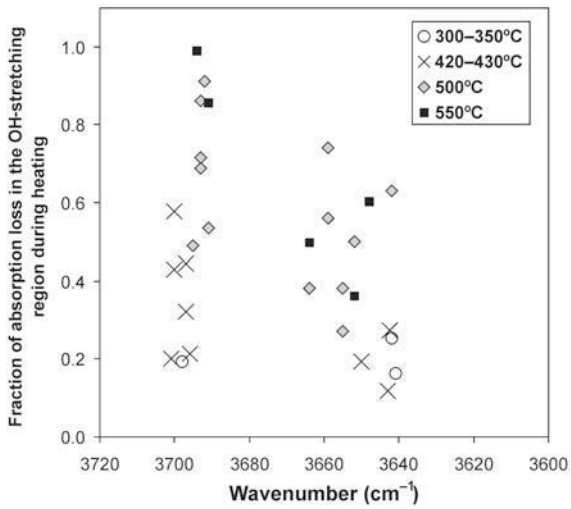

Figure 6. Loss of absorption in the OH-stretching region at several temperatures corresponding to the areas in the subtracted and decomposed spectra (as shown in Figure 5).

spread of the band position values for the ~3660–3640 cm^{-1} region. Another cause is the fact that this region is affected by overlap with the water-hydroxyl band. This overlap made it impossible to obtain more detailed information about K-S dehydroxylation.

OH-bending region. Figure 7 shows an example of the OH-bending region (960–800 cm^{-1}) of a FTIR spectrum (sample TR-117) decomposed into individual metal-OH-metal bands after baseline subtraction. The two bands at 750 and 790 cm^{-1} correspond to another type of molecular interaction and will be addressed later. The remaining bands (thin black lines) are not used here although they are necessary in the curve-fitting calculation. In all studied samples we detected the following OH-bending vibrations, the assignment of which followed a universally accepted scheme for smectite and kaolinite (*e.g.* Russell and Fraser, 1994): 938 cm^{-1} and 916 cm^{-1}: AlAlOH; 870–890 cm^{-1}: AlFeOH; 835 cm^{-1} and 845 cm^{-1}: AlMgOH; 815 cm^{-1}: FeFeOH; 780 cm^{-1}: MgFeOH. There is an additional band at ~895 cm^{-1} that develops with increasing kaolinite content and was assigned to AlAlOH (Frost, 1998).

In Figure 8 we compare the abundance of the three octahedral cations (Al, Mg and Fe) determined from the FTIR and chemical analysis in order to test the reliability of the baseline correction and decomposition technique of the FTIR spectra. The metal abundances are expressed in the form of a 2:1 structure unit-cell, even though this does not have a physical meaning due to the presence of kaolinite, which has a 1:1 structure. (Therefore, the octahedral occupancy for samples with the highest kaolinite content, RS49 and CWP-73, is >4). However, the figures are only considered in their relative values for comparison between chemical and FTIR data. In the case of Mg, the chemical data were corrected for the presence of interlayer Mg. However, the chemical data include tetrahedral as well as octahedral Al, because it is impossible to separate them in K-S. The FTIR cation content was calculated from the areas of the individual bands assuming that all metal-OH-metal vibrations have the same absorptivity. Figure 8a shows that there is a relatively good agreement between the FTIR and chemical assessment of Al content. The typical differences in Al estimations between FTIR and chemical analysis are 0.007–0.62 atoms, yielding 4 to 13% relative error. The agreement is good in spite of the fact that the chemical data include tetrahedral Al, which is not accounted for by FTIR. This is because tetrahedral

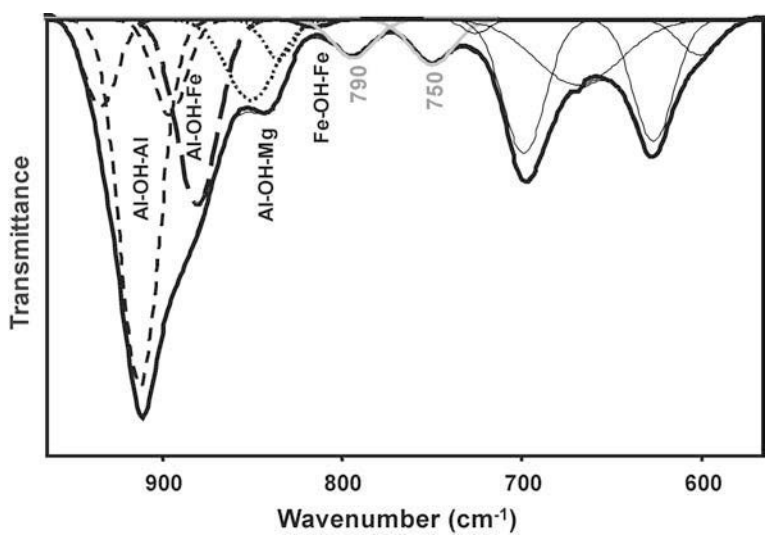

Figure 7. FTIR spectrum of sample TR-117, decomposed into the individual (metal-OH-metal) OH-bending bands (thick black dotted and dashed lines), possible translational vibrations of external OH groups (thick gray lines) and others calculated to obtain a good fit (thin black lines).

https://doi.org/10.1346/CCMN.2006.0540101 Published online by Cambridge University Press

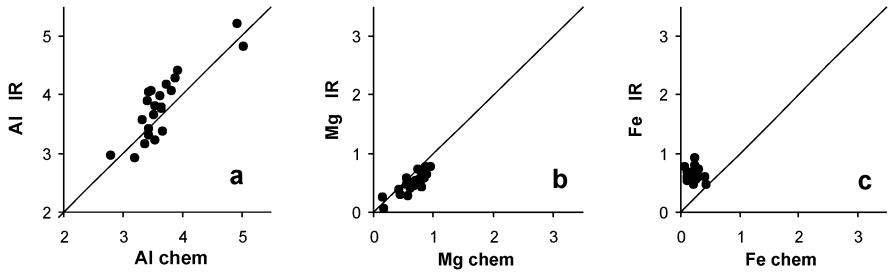

Figure 8. Comparison of the octahedral Al, Mg and Fe content (atoms per formula unit of a hypothetical 2:1 structure) determined by chemical analysis and FTIR. The axes show the same range of values to allow a direct comparison between the plots.

Al is low as shown by the chemical analyses of the smectite end-member of the series. The agreement is also relatively good for Mg (Figure 7b), with slightly greater values for the chemical analysis. The typical differences range from 0.07 to 0.26 atoms, yielding relative errors in the range 8 to 47%. However, FTIR noticeably overestimates Fe abundance with respect to the chemical analysis (Figure 8c). The typical differences range from 0.26 to 0.57 Fe atoms, producing large relative errors from 27 to 493%. We believe that this is mainly due to the difficulties in the accurate quantification of the small FeFeOH band, as the other band contributing to Fe abundance, AlFeOH, does not seem to induce a consistent error in the quantification of Al. Another source of error may have been the selection of the baseline. It seems, therefore, that the applied method of the FTIR spectrum decomposition produced broadly reliable results, with the exception of the FeFeOH band, which is, however, usually very small. In view of this, we decided to use the FTIR data for further analysis.

Figure 9 shows the relative absorption intensities of the OH-bending vibrations of the cation pairs as a function of % K. As expected, the AlAlOH and AlMgOH bands show the opposite trend with progressing kaolinization of smectite, AlAlOH absorption increases and AlMgOH absorption decreases (Figure 9a,b). The intensity of the AlFeOH band shows a slightly decreasing trend with increasing % K (Figure 9c). These three bending vibrations (AlAlOH, AlMgOH and AlFeOH) are the most reliable because their bands are relatively large and well resolved. However, in order to obtain a more complete picture of Mg and Fe behavior during kaolinization, all bands associated with these cations should be considered. The two remaining bands identified in the samples, MgFeOH and FeFeOH are usually small and probably affected by larger relative error; they do not show any trend as kaolinization proceeds (Figure 9d,e). The addition of the FeMgOH and AlMgOH bands causes little change of the trend in Figure 9b. This trend clearly shows the continuous removal of Mg from the K-S structure during kaolinization of smectite. In the case of Fe, however, the addition of the MgFeOH and FeFeOH bands to the AlFeOH band does affect the trend in Figure 9c, causing increased

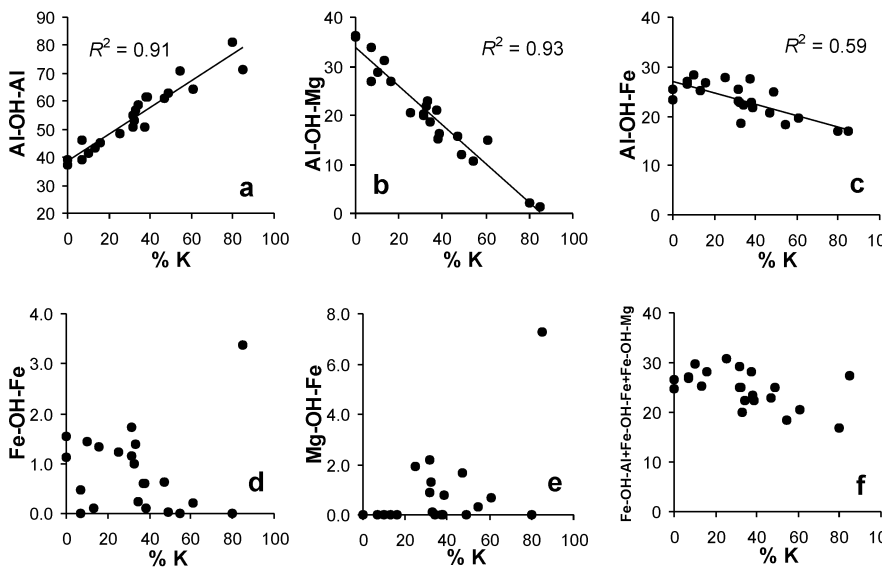

Figure 9. Normalized intensities (% of total OH-bending absorbed intensity) of several metal-OH-metal bending vibrations (a to e), and the sum of all bands involving Fe (f) as a function of % K (% of kaolinite layers). R^2 values correspond to a 95% confidence level.

https://doi.org/10.1346/CCMN.2006.0540101 Published online by Cambridge University Press

spread of the data points (there is no meaningful correlation in Figure 9f). This implies that Fe remains in the structure of the newly formed kaolinite or is removed very slowly as the transformation proceeds, in agreement with our previous conclusions based on chemical analysis. We believe that this is supported by the FTIR data even if the band decomposition method overestimates Fe abundance (Figure 8c), because the data point trend, or the lack of it, depends on the relative intensity values and not on their absolute values. The fact that Fe is retained in the kaolinite layers indicates that kaolinization of smectite proceeds through the inheritance of the original structure.

Figure 10a shows the change of the relative intensity of the band at 750 cm^{-1} with the % K increase in the K-S samples. Farmer (1974) related this band to translational vibrations implicating the external OH groups in kaolinite. Bishop *et al.* (2002) assigned it to out-of-plane OH bending rather than translation, without specifying whether the corresponding OH groups are external. However, as this band is characteristic of kaolinite, it is likely that the OH groups involved are external. This band is coupled in kaolinite with that at 790–795 cm^{-1} (Russell and Fraser, 1994) (see Figure 7); for this analysis, however, we used only the band at 750 cm^{-1} because it appears relatively free from overlap with other bands and it is easier to quantify. The tetrahedral Al-O-Si in-plane vibration band also appears at the same position of 750 cm^{-1} (Farmer, 1974; Russell and Fraser, 1984) but the intensity of this band is very small in smectite and non-existent in kaolinite due to the low or absent tetrahedral Al, and it has very little or no influence on the present analysis. The intensity of the 750 cm^{-1} band was normalized with respect to the sum of all OH-bending bands plus the 750 cm^{-1} band itself.

The plot in Figure 10a shows that the datapoint trend is best approximated by a curve with two inflection points (thin black line: a polynomial regression of the experimental data). This trend has a general shape similar to the equation in Figure 10b, although 'stretched' in the diagonal direction. Figure 10b shows the increase of OH groups in K-S with progressing kaolinization of smectite. The non-linear relation in this plot is interpreted as being due to the development of kaolinite-like patches that collapse to ~7 Å only when they are sufficiently large (see Introduction). The similarity between the trends in Figures 10 a and b suggests that the cause of the intensity increase of the 750 cm^{-1} band is related to the increase in the number of OH groups in K-S, which should be the case if the assignment by Farmer (1974) (and possibly Bishop *et al.*, 2002) is correct. However, since the datapoint trend in Figure 10a does not correspond exactly to that in Figure 10b, we considered the possibility that the intensity of the 750 cm^{-1} band does not depend on the number of external OH groups only. This vibration of external OH groups could be affected by the presence of interlayer cations and water. Neither of the two exists in end-member kaolinite but K-S does have residual interlayer cations in ~7 Å layers, as shown in Figure 10c. If there were no such residual interlayer cations in K-S, Figure 10c would show a linear trend. The residual interlayer cations are probably partially hydrated. Thus, the external OH vibrations considered may very well be affected by the interlayer complex, and the resulting intensity may be diminished. If this is the case, Figure 10a is produced by a combination of the increase in OH groups (Figure 10b) and the decrease in the CEC (Figure 10c), where both effects cooperate in the intensity increase of the 750 cm^{-1} band.

We tested this hypothesis by modeling the datapoint trend in Figure 10a using two components, the regression equation from Figure 10b (equation 1) and the inverse of the regression equation from Figure 10c (equation 2). These equations were modified to make their intercepts equal to zero as no intensity of the investigated band was measured for % K = 0. The equation in the model is $y = a$ (eq. 1) + b (eq. 2), where a and b are two parameters fitted experimentally. The best fit is shown in Figure 10a (thick gray line) and corresponds to the values $a = 1.5$ and $b = 0.15$. The fit is quite good up to 80% kaolinite layers and then departs

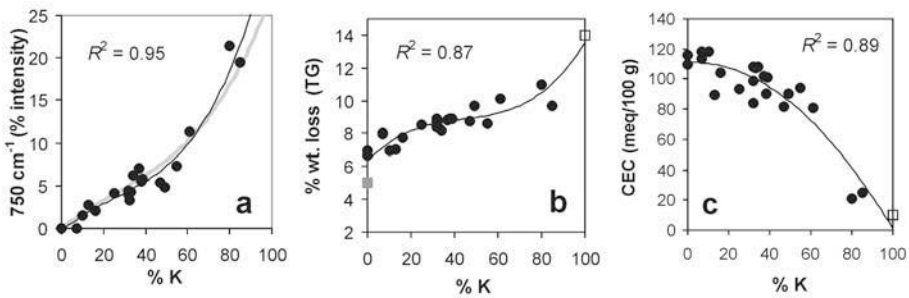

Figure 10. Intensity of the 750 cm^{-1} band (a); percent weight loss due to dehydroxylation of the octahedral sheet (TG analysis) (b); and CEC (c) as a function of % K in K-S (XRD measurements). The thick gray line in (a) was modeled using the regression equations from plots (b) and (c). The thin black line in (a) and the R^2 value correspond to a polynomial regression of the experimental data. Filled gray square: ideal value for smectite; open square: ideal value for kaolinite. All R^2 values correspond to a 95% confidence level.

https://doi.org/10.1346/CCMN.2006.0540101 Published online by Cambridge University Press

from the experimental regression. However, the fact that we only have two experimental values in the region above ~60% kaolinite layers generates some uncertainty about the actual trends in the experimental datasets involved in the model. The values of the parameters *a* and *b* are very different because equation 1 covers a numerical range of values of 11, whereas equation 2 covers a range of 110, *i.e.* 10 times larger. Thus, the fact that *a* is exactly 10 times larger than *b* indicates that the two equations (or the two variables: OH number increase and CEC decrease) have a similar weight in shaping the behavior of the trend in Figure 10a. In our opinion, the assumed effects on the intensity of the 750 cm^{-1} band are very likely and the good fit obtained supports the validity of our interpretation. Interestingly, however, the OH in-plane bending vibrations (938−780 cm^{-1}) do not show the effect of the presence of residual interlayer cations in kaolinite domains. This can best be seen in Figure 9a, where the data point trend is linear. There are two reasons for this: (1) in this case both external and internal OH groups are implicated, and not just the external ones, as in the case of the 750 cm^{-1} band; and (2) the energy and geometry of the OH in-plane bending vibrations are different from those of OH-translation or OH out-of-plane vibrations.

We also investigated the short-range cation ordering in the octahedral sheet by comparison of the FTIR and chemical data. The charts in Figure 11 plot the ratio of the abundance of a selected cation over the sum of all cations from the chemical analysis *vs*. the intensity of a band containing the selected cation divided by the sum of the intensities of all bands involving this cation. Figure 11a evaluates the distribution of the AlAl pairs with respect to AlMg and AlFe. The greater chemical than FTIR ratios indicate that Al tends to mix with Mg and Fe more than occur as AlAl pairs. However, this tendency decreases with increasing kaolinite content as the trend approaches the 45º line, which indicates random distribution of Al in the octahedral sheet. This is expected because as kaolinization proceeds, more Al is incorporated in the octahedral sheet replacing Mg. However, a random Al distribution is not achieved even for samples containing 80% kaolinite. Figures 11b and c show that Mg and Fe mix with Al to a great extent, confirming the result from Figure 11a. Finally, Mg and Fe are segregated from each other, as shown in Figure 11d, except in one case (sample CWP-73), in which they appear to mix to a large extent. The distribution of the FeFe pairs cannot be reliably assessed due to the ambiguous quantification of the FeFeOH band. The results above are not affected by the tetrahedral Al (accounted for in the chemical but not in the FTIR data), which is only a small fraction of the total Al.

In conclusion, it appears that the only change in the octahedral cation ordering of K-S samples during the smectite-to-kaolinite reaction is an increase in the number of the AlAl pairs, as shown by a trend in Figure 11a. The lack of trend in Figures 11b,c and d indicates that Mg and Fe are not rearranged during the reaction. The increment of AlAl pairs results only from the loss of Mg with increasing kaolinization. The Al is not randomly distributed at 80% K possibly because Fe

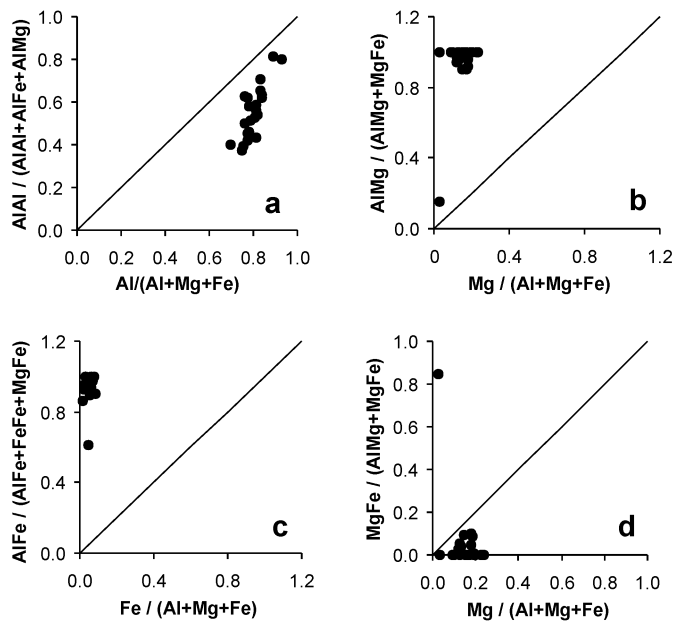

Figure 11. Cation ordering in the octahedral sheet. The plots show the intensity ratio of some individual metal-OH-metal bands to the sum of several metal-OH-metal bands, *vs*. the ratio metal/Al+Mg+Fe from the chemical analysis. Data points on the 45º line indicate a random cation distribution; data above and below the line indicate an abundance of the corresponding metal pair higher and lower than random, respectively.

https://doi.org/10.1346/CCMN.2006.0540101 Published online by Cambridge University Press

is preserved in the structure and AlFe pairs are still very abundant, as indicated in Figure 11c. These observations strongly suggest a solid-state transformation as the mechanism of kaolinization of smectite in these samples.

CONCLUSIONS

(1) The evolution of the intensity of the 750 cm^{-1} band in K-S, possibly corresponding to vibrations implicating external (kaolinite-type) OH groups, with progressing kaolinization is controlled by the number of external OH groups in kaolinite domains, as expected, but also by residual interlayer cations (possibly hydrated). If the assignment of the band is correct, this result indicates that residual layer charge is preserved in the kaolinite domains.

(2) During the smectite-to-kaolinite reaction, the intensities of the FTIR bands involving Mg decreases sharply whereas the intensity of the bands related to Fe do not show any trend. This is in agreement with the chemical data showing Mg loss and Fe retention in K-S with proceeding kaolinization.

(3) Analysis of short-range ordering in K-S octahedral sites indicates that atoms are not rearranged during smectite-to-kaolinite conversion, except that there is a decrease in AlMg pairs and an increase in AlAl pairs produced by Al-for-Mg substitution.

(4) These conclusions point to solid-state transformation as the most likely mechanism of kaolinization of smectite, in agreement with previous studies based on XRD, TG, chemical analysis and NMR.

ACKNOWLEDGMENTS

We thank Stephen Hillier for providing one of the samples, Andreas Morlok for assistance with the FTIR analyses, Royal Society/NATO (grant 15144/02B/TB) and the Marie Curie programme of the European Community (contract MEIF-CT-2003-501678) for financial support. We also thank Jana Madejová, an anonymous reviewer and Peter Komadel for their comments on the manuscript.

REFERENCES

Bishop, J., Murad, E. and Dyar, M.D. (2002) The influence of octahedral and tetrahedral cation substitution on the structure of smectite and serpentines as observed through infrared spectroscopy. *Clay Minerals*, **37**, 617–628.

Brindley, G.W. (1980) Order-disorder in clay mineral structures. Pp. 125–196 in: *Crystal Structures of Clay Minerals and their X-ray Identification* (G.W. Brindley and G. Brown, editors). Monograph **5**, Mineralogical Society, London.

Brown, G. and Brindley, G.W. (1980) X-ray diffraction procedures for clay mineral identification. Pp. 305–360 in: *Crystal Structures of Clay Minerals and their X-ray Identification* (G.W. Brindley and G. Brown, editors). Monograph **5**, Mineralogical Society, London.

Churchman, G.J., Slade, P.G., Self, P.G. and Janik, L.P. (1994) Nature of interstratified kaolin-smectites in some Australian soils. *Australian Journal of Soil Research*, **32**, 805–822.

Cuadros, J., Delgado, A., Cardenete, A., Reyes, E. and Linares, J. (1994) Kaolinite/montmorillonite resembles beidellite. *Clays and Clay Minerals*, **42**, 643–651.

Delvaux, B., Mestdagh, M.M., Vielvoye, L. and Herbillon, A.J. (1989) XRD, IR and ESR study of experimental alteration of Al-nontronite into mixed-layer kaolinite-smectite. *Clay Minerals*, **24**, 617–630.

Delvaux, B., Herbillon, A.J., Vielvoye, L. and Mestdagh, M.M. (1990) Surface properties and clay mineralogy of hydrated halloysitic soil clays. II: Evidence for the presence of halloysite/smectite (H/Sm) mixed-layer clays. *Clay Minerals*, **25**, 141–160.

Dudek, T., Cuadros, J. and Fiore, S. (2006) Interstratified kaolinite-smectite: nature of the layers and mechanism of smectite kaolinization. *American Mineralogist*, **91**, 159–170.

Farmer, V.C. (1974) The layer silicates. Pp. 331–363 in: *The Infrared Spectra of Minerals* (V.C. Farmer, editor). Monograph **4**, Mineralogical Society, London.

Frost, R.L. (1998) Hydroxyl deformation in kaolins. *Clays and Clay Minerals*, **46**, 280–289.

Hillier, S., Price, R. and Roe, M. (2002) Mixed-layer kaolinite-smectite from the Jurassic Blisworth Clay, Northamptonshire. *18th General Meeting of International Mineralogical Association*, 2002, Edinburgh, Scotland, Abstracts and Program, p. 165.

Jackson, M.L. (1975) *Soil Chemical Analysis – Advanced Course* (M. Jackson, editor). University of Wisconsin, Madison, USA.

Linares, J. (1985) The process of bentonite formation in Cabo de Gata, Almeria, Spain. *Mineralogica et Petrographica Acta*, **29-A**, 17–33.

Madejová, J., Keèké, J., Pálková, H. and Komadel, P. (2002) Identification of components in smectite/kaolinite mixtures. *Clay Minerals*, **37**, 377–388.

Reyes, E., Huertas, F. and Linares, J. (1978) [Génesis y geoquímica de las esmectitas de Andalucía (España)]. Genesis and geochemistry of the smectites of Andalucia (Spain). *Proceedings of the 1st International Congress on Bentonites,* Sassari-Calgari, Italy, pp. 149–176.

Reynolds, R.C. Jr. and Reynolds, R.C., III (1996) *NEWMOD: The calculation of one-dimensional X-ray diffraction patterns of mixed-layer clay minerals*. Computer Program. 8 Brook Road, Hanover, New Hampshire, USA.

Russell, J.D. and Fraser, A.R. (1994) Infrared methods. Pp. 11–67 in: *Clay Mineralogy: Spectroscopic and Chemical Determinative Methods* (M.J. Wilson, editor). Chapman & Hall, London.

Schultz, L.G., Shepard, A.O., Blackmon, P.D. and Starkey, H.C. (1971) Mixed-layer kaolinite-montmorillonite from the Yucatan Peninsula, Mexico. *Clays and Clay Minerals*, **19**, 137–150.

Smith, B.F.L. (1994) Characterization of poorly ordered minerals by selective chemical methods. Pp. 333–358 in: *Clay Mineralogy: Spectroscopic and Chemical Determinative Methods* (M.J. Wilson, editor). Chapman & Hall, London.

Środoń, J. (1980) Synthesis of mixed-layer kaolinite/smectite. *Clays and Clay Minerals*, **26**, 419–424.

Theng, B.K.G., Churchman, G.J. and Whitton, J.S. (1984) Comparison of intercalation methods for differentiating halloysite from kaolinite. *Clays and Clay Minerals*, **32**, 249–258.

Watanabe, T., Sawada, Y., Russell, J.D., McHardy, W.J. and Wilson, M.J. (1992) The conversion of montmorillonite to interstratified halloysite-smectite by weathering in the Omi acid clay deposit, Japan. *Clay Minerals*, **27**, 159–173.

(*Received 7 March 2005; revised 11 August 2005; Ms. 1022; A.E. Peter Komadel*)